ORIGINAL RESEARCH

Lightweight, flexible, and multifunctional anisotropic nanocellulose-based aerogels for CO_2 adsorption

Jiayuan Wei · Shiyu Geng · Jonas Hedlund · Kristiina Oksman

Abstract CO_2 adsorption is a promising strategy to reduce costs and energy use for CO_2 separation. In this study, we developed CO_2 adsorbents based on lightweight and flexible cellulose nanofiber aerogels with monolithic structures prepared via freeze-casting, and cellulose acetate or acetylated cellulose nanocrystals (a-CNCs) were introduced into the aerogels as functional materials using an impregnation method to provide CO_2 affinity. The microstructure of the adsorbent was examined using scanning electron microscopy, and compression tests were performed to analyze the mechanical properties of the adsorbents. The CO_2 adsorption behavior was studied by recording the adsorption isotherms and performing column breakthrough experiments. The samples showed excellent mechanical performance and had a CO_2 adsorption capacity of up to 1.14 mmol/g at 101 kPa and 273 K. Compared to the adsorbent which contains cellulose acetate, the one impregnated with a-CNCs had better CO_2 adsorption capacity and axial mechanical properties owing to the building of a nanoscale scaffold on the surface of the adsorbent. Although the CO_2 adsorption capacity could be improved further, this paper reports a potential CO_2 adsorbent that uses all cellulose-based materials, which is beneficial for the environment from both resource and function perspectives. Moreover, the interesting impregnation process provides a new method to attach functional materials to aerogels, which have potential for use in many other applications.

Keywords Cellulose aerogel · CO_2 adsorption · Freeze-casting · Cellulose nanocrystals · Acetylation

J. Wei · S. Geng · K. Oksman
Division of Material Science, Department of Engineering Sciences and Mathematics, Luleå University of Technology, 97 187 Luleå, Sweden

J. Hedlund
Chemical Technology, Department of Civil, Environmental and Natural Resources Engineering, Luleå University of Technology, 97 187 Luleå, Sweden

K. Oksman
Fibre and Particle Engineering, University of Oulu, 90014 Oulu, Finland

K. Oksman (✉)
Mechanical and Industrial Engineering (MIE), University of Toronto, Toronto, ON M5S 3G8, Canada
e-mail: kristiina.oksman@ltu.se

Introduction

Adsorption is an energy-efficient and low cost method for capturing CO_2 (Pino et al. 2016; Yu et al. 2012). A suitable CO_2 adsorbent should have a high specific surface area, a high porosity with proper pore sizes, a

favorable surface chemistry, and a high chemical/mechanical stability. Many CO_2 adsorbents based on different materials, such as zeolites (Banerjee et al. 2009; Cavenati et al. 2004; Kongnoo et al. 2017; Ojuva et al. 2013), silica gels (Arellano et al. 2016), activated carbon (Fujiki and Yogo 2016; Roberts et al. 2017; Singh et al. 2017), and metal-organic frameworks (An and Rosi 2010; Millward and Yaghi 2005; Salehi and Anbia 2017), have been investigated in recent decades. However, adsorbents based on these materials have some drawbacks, such as their high cost, complex preparation methods, toxicities, and the use of corrosive materials during their preparation. Therefore, researchers continue to look for some new materials to produce CO_2 adsorbents that could be used on the industrial scale.

Biomass-derived materials have attracted attention owing to their abundant resources, renewability, and biodegradability (Jonoobi et al. 2014; Khalil et al. 2012; Oksman et al. 2003). Nanocellulose materials, including cellulose nanofibers (CNFs) and cellulose nanocrystals (CNCs), that can be extracted from various types of biomass have attracted considerable interest owing to their specific physical and chemical properties (Geng et al. 2018; Herrera et al. 2017; Nissilä et al. 2019). Recently, several studies on the preparation of highly porous nanocellulose-based aerogels using ice-templating have been reported, and some have shown interesting adsorption/absorption capabilities. In an adsorption process, gas or liquid molecules are captured on the surface of the adsorbents while in an absorption process, those molecules can enter the bulk of the absorbents and create strong interactions there (Yu et al. 2012). Yang et al. (2018) prepared aerogels containing CNFs and sodium alginate using unidirectional and bidirectional ice-templating. They found that after silane modification, the obtained aerogel was superoleophilic, which have oil absorption capacities up to 34 times its weight. Using similar techniques, Zhang et al. (2019) also reported CNF-based aerogel for selective oil/organic solvent absorption. The aerogels shown outstanding compression flexibility and high hydrophobicity which allowed the aerogels to absorb oils that were 99 times of its weight. Gorgieva *et al.* reported a unidirectionally ice-templated cationic dye remover prepared from carboxymethyl cellulose and CNFs with the highest dye adsorption capacity of approximately 1.8 g/g adsorbent (Gorgieva et al. 2019).

Valencia et al. (2019) prepared hybrid aerogels consisting of CNFs, gelatin and zeolite for CO_2 adsorption via unidirectional freeze-casting. The aerogel containing 85 wt% zeolite showed an CO_2 adsorption capacity of approximately 1.2 mmol/g at 308 K and 101 kPa.

Although these previous studies illustrate that nanocellulose materials can form highly porous structures with large surface areas, which is beneficial for adsorption, pure nanocellulose does not have good affinity to CO_2 molecules (Gebald et al. 2011). Thus, the sorbent–sorbate affinity needs to be improved to produce a nanocellulose-based CO_2 adsorbent that can adsorb CO_2 from a mixed gas. It has been reported that some polar groups such as nitriles (–CN), carbonyls (–C=O–), acetates (–COO–), and amides (–NHCO–) contribute to a high CO_2 solubility and CO_2/N_2 selectivity (Park and Lee 2008). There have been several studies on the functionalization of cellulose by amine groups to improve the cellulose–CO_2 affinity. Gebald et al. (2011) synthesized amine-based CO_2 adsorbents composed of CNFs and N-(2-aminoethyl)-3-aminopropylmethyldimethoxysilane, where the highest adsorption capacity achieved was 1.39 mmol/g after 12 h. Subsequently, they found that amine-functionalized nanocellulose provided a stable CO_2 adsorption capacity (approximately 0.9 mmol/g) in ambient air during adsorption/desorption cycling tests (Gebald et al. 2013). However, in addition to an enhanced CO_2 adsorption capacity, amine-based materials require a relatively large amount of energy to regenerate adsorbed CO_2 (Gebald et al. 2011), which is an obstacle to using this kind of adsorbent on a large scale. Under this circumstance, acetyl groups could be an alternative. Kilic et al. (2007) experimentally confirmed that acetate-functionalized polymers are more CO_2-soluble than polymers with only ether groups because the addition of an ester oxygen provides a much stronger attractive site than that of the ether group for CO_2 interactions. Moreover, the oxygen of carbonyl groups is more electron-rich and more favorable for CO_2 binding. Karimi et al. (2016) functionalized silica membranes with acetyl groups and reported that the CO_2 adsorption was increased compared to that of the unmodified membranes.

Inspired by the previous studies on nanocellulose-based aerogels and acetate-based materials for CO_2 adsorption, in this study, we demonstrated a novel

method to prepare lightweight and flexible nanocellulose-based CO_2 adsorbents with functional acetate groups and anisotropic structures. The adsorbents consist of a freeze-cast CNF aerogel and acetylated CNCs in which the acetylated CNCs were attached in the anisotropic porous CNF aerogel by an impregnation process driven by capillary forces. The acetylated CNCs have a certain amount of acetyl groups on the surface; however, the integrity of CNCs is maintained. Thus, they are expected to build nanoscale scaffolds together with the CNF aerogel, which is beneficial for the CO_2 adsorption capacity. Cellulose acetate was used as the reference, which was also attached to the CNF aerogel by impregnated with different amounts. The structure and morphology of the materials and the prepared adsorbents were investigated, and the mechanical properties and CO_2 adsorption capacity of the adsorbents were examined and discussed.

Experimental section

Materials

The aqueous CNF dispersion with a solid content of 1 wt% was mechanically separated from birch pulp using a Masuko grinder (Japan); the birch pulp was kindly provided by Svenska Cellulosa AB, Piteå, Sweden. The aqueous CNC dispersion (2013-FPL-CNC-049, a solid content of 10.3 wt% in which 1.02 wt% was sulfate ester groups on dry CNCs) was kindly provided by the USDA Forest Service. Acetic anhydride ($\geq$ 99.0%, Fluka, Germany), sodium thiosulfate (99%, Sigma-Aldrich, Germany), ethanol (99.5%, Solveco, Sweden), acetone (Analytical grade, Solveco, Sweden), iodine (> 99%, Alfa Aesar, Germany), cellulose acetate (average Mn $\sim$ 30,000 by GPC, Sigma-Aldrich, USA), sodium hydroxide solution (0.1 N standardized solution, Alfa Aesar, Germany), hydrochloric acid solution (0.5 N standardized solution, Alfa Aesar, Germany), phenolphthalein (ACS reagent, Sigma-Aldrich, Germany), 1,2,3,4-butanetetracarboxylic acid (BTCA, 99%, Sigma-Aldrich, India), and potassium bromide (FT-IR grade, Alfa Aesar, Germany) were purchased and used without further purification.

Sample preparation

Preparation of the CNF aerogel

First, 62 g of 1 wt% CNF aqueous suspension was mixed with 0.03 g of BTCA (as a crosslinker) by stirring for 1 h at room temperature. The mixture was then frozen unidirectionally by a freeze-casting setup with a freezing rate of 5 K/min (Deville et al. 2006) and freeze-dried for 72 h at a pressure of 0.064 mbar using a freeze dryer (Alpha 1–2 LD plus, Martin Christ GmbH, Germany). All the freeze-dried samples were placed in a vacuum oven at 393 K for 3 h to crosslink the aerogel via esterification between CNFs and BTCA. Finally, the crosslinked CNF aerogel was obtained for further processing.

Acetylation of cellulose nanocrystals

The acetylation method used in this study is based on a heterogeneous process that uses iodine as a catalyst (Abraham et al. 2016). Briefly, solvent exchange of the CNC suspension from water to acetic anhydride (Ac_2O) through acetone was carried out prior to the modification. A CNC/Ac_2O suspension with a concentration of 0.02 g/mL of CNC in Ac_2O was prepared and heated to 373 K for 1 h. Iodine (0.001 g/mL of I_2 in Ac_2O) was added as a catalyst, and the reaction ran for another 30 min. Subsequently, the suspension was cooled to room temperature, and saturated sodium thiosulphate solution was added dropwise until the color of the reactant changed from brown to transparent to stop the reaction. The mixture was poured into ethanol/water (weight ratio of 2:1) and stirred for 30 min to precipitate the acetylated CNCs (a-CNC). The precipitated a-CNCs was then further washed with ethanol (70 vol%) and distilled water. Finally, a-CNCs was collected and dispersed in acetone to make a homogenous suspension for impregnation.

Impregnation of the aerogels

First, 40 g of the a-CNC/acetone suspension at a concentration of 0.25 wt% was used for impregnation, and the same amounts of cellulose acetate/acetone solution with 0.25 wt% and 1.25 wt% of solid contents, respectively, were prepared as references. The crosslinked CNF aerogel was placed vertically in the suspension/solution until the suspension/solution

was completely adsorbed by the aerogel owing to the capillary force (Movie S1, Supporting Information, SI). Because all the 40 g of the solution/suspension was impregnated into the CNF aerogel, the amount of the a-CNCs/cellulose acetate added is controlled by the concentration of the solution. The impregnated aerogel was then placed in the vacuum oven at 368 K overnight to remove acetone. The weight of the aerogel was measured before and after the impregnation process to calculate the amount of a-CNC or cellulose acetate that had been attached to the sample. The sample coding and the compositions of all samples prepared for this study are shown in Table 1.

Characterization

Atomic force microscopy (AFM)

AFM was used to characterize the morphology of the CNFs used in this study. To prepare the AFM sample, the CNF suspension was diluted to 0.001 wt% of solid content, and then, a droplet was deposited on freshly cleaved mica and dried at room temperature. The sample was scanned using a Veeco MultiMode scanning probe (Santa Barbara, USA) in tapping mode. The width of the CNFs was measured according to the height in the AFM height images. More than 80 nanofibers were analyzed, and the average fiber width was then calculated.

Fourier transform infrared spectroscopy (FT-IR)

FT-IR was used to study the crosslinking of the CNF aerogel and the acetylation of the CNCs. To prepare the FT-IR samples, the crosslinked CNF aerogel was washed thoroughly with distilled water to remove the possible unreacted BTCA and then grounded and dried

in a vacuum oven at 393 K. The filtered a-CNCs were also dried in the vacuum oven overnight prior to the FT-IR test. The uncrosslinked CNF aerogel and unacetylated CNCs were prepared in the same manner for comparison. Then, 30 mg of the sample was carefully mixed and pressed with 270 mg of KBr and then tested using a Vertex 80v FT-IR spectrometer (Bruker, USA). For each single experiment, 128 scans were run at a resolution of 4 cm^{-1}.

Titration

The degree of substitution (DS) of the prepared a-CNCs was measured by titration according to ASTM D871-96 (Zhou et al. 2016). Briefly, 0.1 g of dried a-CNCs were dispersed in 40 mL of 70 vol% ethanol at 60 °C for 30 min; then, 40 mL of 0.1 N NaOH was added. The mixture was stirred for 15 min; then, it stood at room temperature for 48 h with occasional shaking. Phenolphthalein was used as a pH indicator, and 0.5 N HCl was used to titrate the mixture until the color changed from pink to faint pink. The unacetylated CNC was titrated as a blank using the same method, and the DS of the a-CNCs was calculated using the following equations (Ramírez et al. 2017):

$$DS = \frac{162 \times Acyl\%}{4300 - (42 \times Acyl\%)} \tag{1}$$

$$Acyl\% = \frac{(V_b - V_s) \times N_{HCl} \times 43}{W \times 1000} \times 100\% \tag{2}$$

where Acyl% denotes the acyl group content. V_b and V_s represent the volumes of HCl added to the blank and to the a-CNC sample, respectively. N_{HCl} corresponds to the normality of the HCl solution, which was 0.5 N. W is the mass of the used sample.

Table 1 Sample coding and compositions of the samples prepared for this study

Sample code[a]	Impregnated material	Amount of the impregnated material (g)
CNF-X	N/A	0
CNF-X-0.1CA	Cellulose acetate	0.1
CNF-X-0.5CA	Cellulose acetate	0.5
CNF-X-a-CNC	Acetylated CNCs	0.07

[a]All samples were crosslinked, and "X" stands for "crosslinking"

Porosity measurement

The porosity of the prepared aerogels was calculated as (Sehaqui et al. 2011):

$$P = 1 - \frac{\rho^*}{\rho} \qquad (3)$$

where the density of the aerogel, ρ^*, was calculated by dividing the weight of the aerogel by its volume. The density of the solid material, ρ, was calculated as:

$$\rho = \frac{1}{\frac{\omega_c}{\rho_c} + \frac{\omega_A}{\rho_A} + \frac{\omega_B}{\rho_B}} \qquad (4)$$

where ω_c, ω_A and ω_B denote the weight percentages of CNFs, the impregnated material (cellulose acetate or a-CNCs), and BTCA, respectively. ρ_c, ρ_A and ρ_B correspond to the solid densities of cellulose, the impregnated material, and BTCA respectively, which were 1.46 g/cm³, 1.28 g/cm³, and 1.65 g/cm³ (Sehaqui et al. 2011).

Scanning electron microscopy (SEM)

The morphology of the aerogels was investigated using a scanning electron microscope (JSM-IT300 InTouchScope, JEOL, Japan). Samples were cut by a sharp blade that was perpendicular and parallel to the freezing direction, respectively. The cut surfaces were coated with gold using a Leica EM ACE200 coater (Wetzlar, Germany) prior to the observation to avoid charging, and the secondary electron images were captured.

Brunauer–Emmett–Teller (BET) surface area

The BET surface area was measured using a BET analyzer (Gemini VII 2390a, Micromeritics Instrument Corp., Norcross, USA). The samples were degassed at 368 K for 24 h under vacuum before the BET surface area measurements were performed.

Compression testing

The mechanical properties of the aerogels were examined by compression testing using a Q800 dynamic mechanical analyzer (TA Instruments, USA) with the compression configuration. Samples were cut into a 1-cm cubic geometry and tested in both axial and radical directions. The experiment was carried out when equilibrated at 303 K with a 0.01 N preload and a strain rate of 10%/min. The elastic modulus (E) of the sample was calculated according to the slope of the initial linear part of the stress–strain curve, and the specific elastic modulus (E_s) of the samples was calculated as shown below:

$$E_s = \frac{E}{\rho^*} \qquad (5)$$

CO_2 adsorption measurement

The capacity for CO_2 adsorption of the impregnated aerogels was studied using a BET analyzer (ASAP 2020 Plus, Micromeritics Instrument Corp., Norcross, USA) as a function of pressure. Approximately 20 mg of the sample was loaded and degassed at 393 K for 24 h, and the degassed sample was precisely weighed and transferred back to the analyzer. The CO_2 isotherm was then measured at 273 K in a pressure range of 0–101 kPa. The CO_2 forward-step change break-through curve of the aerogels was determined by loading the sample in a steel column (15 mm in inner diameter, 300 mm in length). The sample was first treated under a 0.5 L/min nitrogen flow at 368 K for 24 h. After cooling, a mixture of N_2/CO_2 with 10% CO_2 (AGA Gas AB, Sweden) was fed at a flow rate of 0.3 L/min at room temperature. The CO_2 concentration was monitored by an IR 1507 fast-response CO_2 infrared transducer (CA-10 Carbon Dioxide Analyzer–Sable Systems International, USA).

Results and discussion

The morphology of the CNFs used to prepare the CNF aerogel was characterized by AFM, as illustrated in Fig. 1a. Their width distribution is shown in Fig. 1b, and the average width was determined to be 8.5 ± 6.1 nm. The CNCs used for acetylation were fully characterized in our previous study with a width of 5.0 ± 1.5 nm and a length of 122.6 ± 53.3 nm (Butylina et al. 2016). As reported by Kilic et al. (2007), polymers containing acetate groups have a considerable higher CO_2 solubility than those with only ether functionalities because the acetate groups have three binding modes that can interact with CO_2
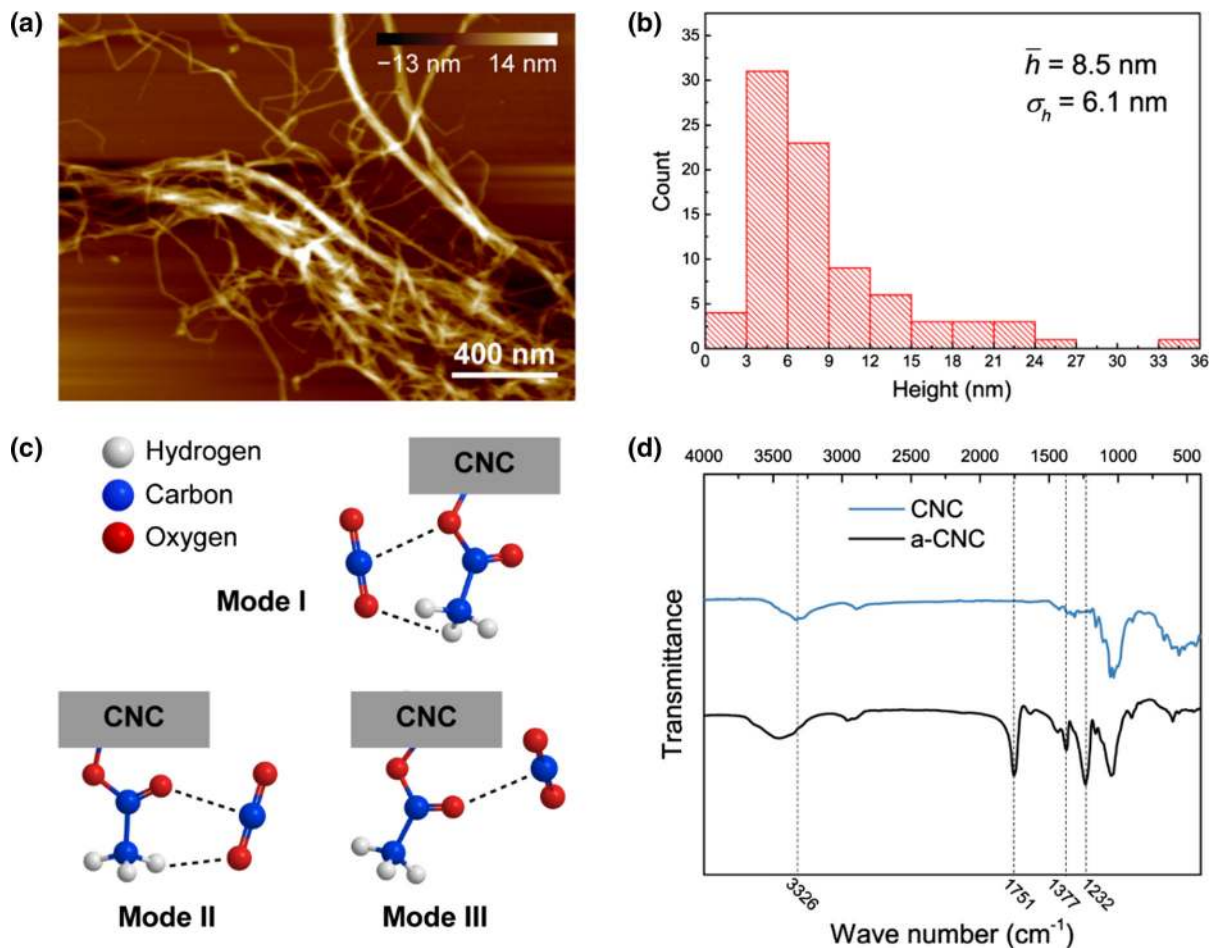
Fig. 1 **a** AFM height image of the CNFs used in this study. **b** The width distribution histogram of the CNFs obtained from their AFM height images. **c** The three binding modes between the a-CNCs and CO₂ molecules. **d** FT-IR spectra of native CNCs and a-CNCs

molecules, i.e. two with a carbonyl oxygen and one with an ester oxygen, as shown in Fig. 1c. Thus, the acetylated CNCs were prepared in this study as the functional materials for CO_2 adsorption. The successful acetylation was confirmed using FT-IR, as illustrated in Fig. 1d. Three peaks are commonly used to identify the acetate group. The carbonyl stretching vibration is at 1751 cm^{-1} (C=O), the C–H in-plane bending of –CO–CH₃ is at 1377 cm^{-1} and the stretching of C–O in the acetyl group (–COO–) is at 1232 cm^{-1} (Hu et al. 2011; Uschanov et al. 2011). The prominent peaks for the a-CNC sample indicate that heterogeneous acetylation was successful. No other adsorption was observed between 1840 and 1760 cm^{-1}; and therefore, there was no unreacted acetic anhydride left. The absence of the carboxylic group peak at 1700 cm^{-1} indicated no acetic acid

byproducts (Hu et al. 2011). The degree of substitution of the a-CNCs was determined to be 1.6 by titration.

After the preparation of the CNF aerogel via freeze-casting and freeze-drying, the CNF aerogel was crosslinked with BTCA and then impregnated with an a-CNCs/acetone suspension or cellulose acetate/acetone solution to prepare the CO_2 adsorbents. The entire procedure is shown schematically in Fig. 2. The crosslinking process was performed to strengthen the CNF aerogel to help it maintain intact during the impregnation process. Figure 3a shows the FT-IR spectra of the CNF aerogel before and after crosslinking. A new adsorption peak appeared in the cross-linked sample at 1730 cm^{-1}, which corresponded to carbonyl stretching (C=O) in the ester group. It suggests that ester groups were formed between the
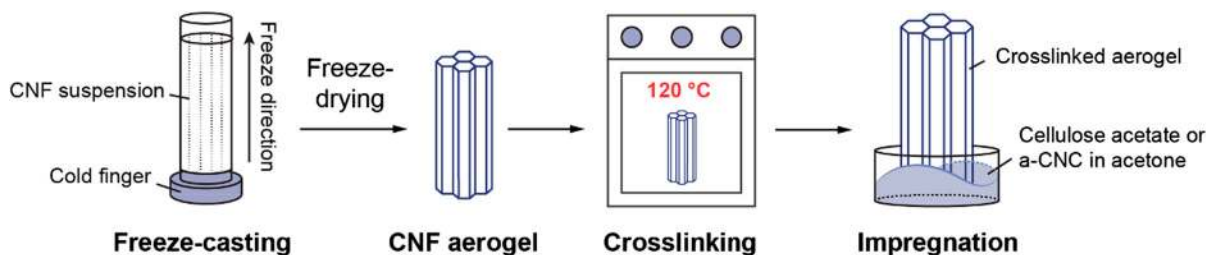
Fig. 2 Process of preparing the acetate-functionalized nanocellulose-based CO_2 adsorbents used in this study
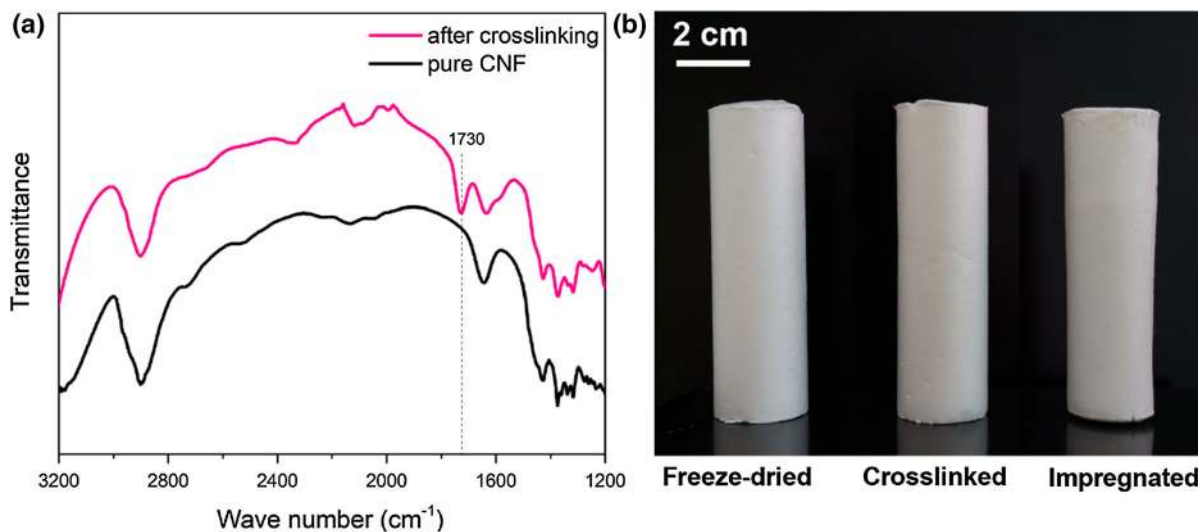

Fig. 3 **a** FT-IR spectra of the native CNF aerogel and crosslinked CNF aerogel and **b** illustration of the aerogels after freeze-drying, crosslinking, and the impregnation process

hydroxyl groups of CNFs and the carbonyl groups of BTCA (Chen et al. 2016; Kono and Zakimi 2013).

The impregnation process is a simple yet robust method to attach functional materials to aerogels that we developed in this study. Movie S1 shows a representative impregnation experiment. Driven by capillary forces, the to be impregnated material can be adsorbed by the CNF anisotropic aerogel in a couple of seconds depends on the length of the aerogel and the viscosity of the impregnated material. Moreover, we demonstrate that not only the polymer solutions (cellulose acetate) but also the nanoparticle suspensions (a-CNCs) can be impregnated, which provides a unique method to produce porous materials with special functionalities. Finally, a CO_2 adsorbent with a length as long as 10 cm can be obtained after drying, and there is no obvious shrinkage in the aerogels after the impregnation with 0.1 g CA, as illustrated in

Fig. 3b. The aerogel impregnated with 0.5 g CA shrank a bit more due to the increase in the viscosity of the impregnating solution. However, the cylindrical shape of the aerogel was remained. The density, porosity, and specific surface area of the prepared adsorbents are shown in Table 2. The porosities of all the adsorbents are higher than 98%. The specific surface area of CNF-X-a-CNC reached 21.04 m^2/g, which was higher than CNF-X-0.1CA, and higher than that of CNF-X-0.5CA, which is the lowest likely owing to the relatively large amount of impregnated cellulose acetate (0.5 g) filled part of the pores in the CNF aerogel.

The microstructure of the adsorbents was investigated by SEM and is shown in Fig. 4. It is obvious from Fig. 4a_i–d_i and Fig. 4a_{ii}–d_{ii} that all adsorbents have a distinct monolithic structure with anisotropic pores, which is formed during the freeze-casting

Table 2 Density, porosity, and the specific surface area of the samples

Sample	ρ^* (kg/m^3)	Porosity (%)	Specific surface area (m^2/g)
CNF-X	12.49 ± 0.37	99.15 ± 0.02	22.47
CNF-X-0.1CA	14.89 ± 0.12	98.97 ± 0.01	17.84
CNF-X-0.5CA	23.50 ± 0.01	98.30 ± 0.01	14.66
CNF-X-a-CNC	16.65 ± 0.96	98.85 ± 0.05	21.04
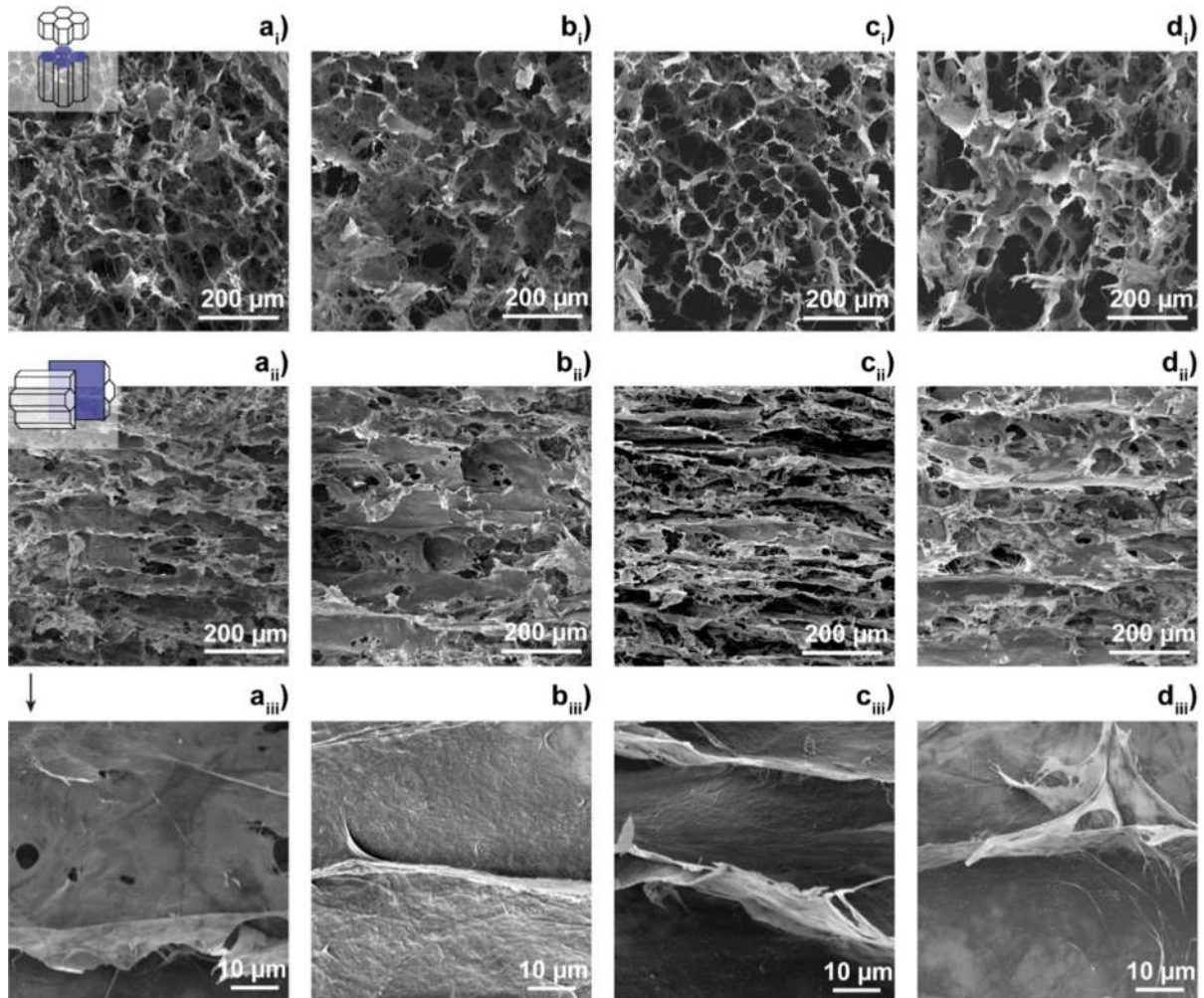
Fig. 4 SEM images of **a** CNF-X, **b** CNF-X-0.1CA, **c** CNF-X-0.5CA, and **d** CNF-X-a-CNC. a_i–d_i The cross-section of the samples prepared perpendicularly to the freezing direction. a_{ii}– d_{ii} The cross-section of the samples prepared parallel to the freezing direction. a_{iii}–a_{iii} Magnified images of the samples from the parallel cross section

process owing to the preferred growth of ice crystals when frozen unidirectionally (Lee and Deng 2011). Typically, in the CO_2 adsorption process, gas containing CO_2 will pass through columns filled with adsorbents. Therefore, the microstructure of the adsorbent is important to ensure a rapid and smooth

adsorption process. It is reported that the monolithic structure has potential advantages in CO_2 adsorption applications because of the improved mass-transfer, low pressure drop at high flow rates and uniform flow distribution (Rezaei and Webley 2010; Svec and Huber 2006). In Fig. 4, there was no collapse of the

pores observed in the impregnated adsorbents, indicating that the impregnation process did not damage the anisotropic structure. However, the width of the pores in CNF-X-0.5CA (Fig. 4c_ii) showed a decreasing trend compared to that of the pores in CNF-X (Fig. 4a_ii) and CNF-X-0.1CA (Fig. 4b_ii). This phenomenon may be a result of the increase in viscosity of the impregnation solution. With an increase in the amount of cellulose acetate dissolved in a certain amount of acetone, the impregnation solution containing 0.5 g of cellulose acetate became more viscous than the one containing 0.1 g of cellulose acetate. Therefore, CNF-X-0.5CA suffered more of a pressure gradient when dried in the oven, which led to a decrease in the pore width. Comparing the magnified images of CNF-X (Fig. 4a_iii) with the impregnated adsorbents, the cell walls of aerogels impregnated with cellulose acetate (Fig. 4b_iii and Fig. 4c_iii) were more compact than that of CNF-X, suggesting that small pores on the cell wall of CNF-X may be filled with cellulose acetate during the impregnation process. Such a filling effect is much less prominent in CNF-X-a-CNC (Fig. 4d_iii), which corresponds to the specific surface area results (Table 2). Instead of filling up small pores on the cell wall, the a-CNCs could build a nanoscale scaffold together with the CNF aerogel owing to their integrity, which is beneficial for the CO_2 adsorption properties.

The mechanical properties of the adsorbents were characterized by compression tests. The resulting stress–strain curves in both the axial and radial

directions are illustrated in Fig. 5, and the E, E_s, and yield strength data of the adsorbents in the axial direction are shown in Table 3. The stress–strain curves in the axial direction shown in Fig. 5a display the typical compression behavior of foams, including linear elastic, plateau, and densification regions. Owing to equipment limitations (maximum load is 18 N), the CNF-X-0.5CA and CNF-X-a-CNC experiments could not reach the same strain as those of CNF-X and CNF-X-0.1CA. Compared to those of CNF-X, both E and the yield strength of the aerogels were enhanced after impregnated with cellulose acetate. The E was 9% and 60% higher by impregnated with 0.1 g and 0.5 g cellulose acetate, respectively. This enhancement is attributed to the higher integrity of the cell walls in the impregnated aerogels. Interestingly, CNF-X-a-CNC demonstrated the highest E (328.9 kPa) and E_s (19.8 kNm/kg) among all the samples with a relatively low amount of impregnated a-CNCs (0.07 g), indicating that the a-CNCs provided a remarkable reinforcing effect caused by the very high rigidity of the CNCs. Moreover, the E_s of CNF-X-a-CNC outperformed previously reported cellulose-based aerogels (4–18 kNm/kg) (Fan et al. 2018; López Durán et al. 2018; Zhang et al. 2019), and it was in the range of expanded polystyrene and polyurethane foams (10–100 kNm/kg) (Gibson and Ashby 1999). Figure 5b shows the compression behavior of the samples in the radial direction, and there was no significant difference observed. All the samples showed very high flexibility, and their elastic strain could reach 60%.
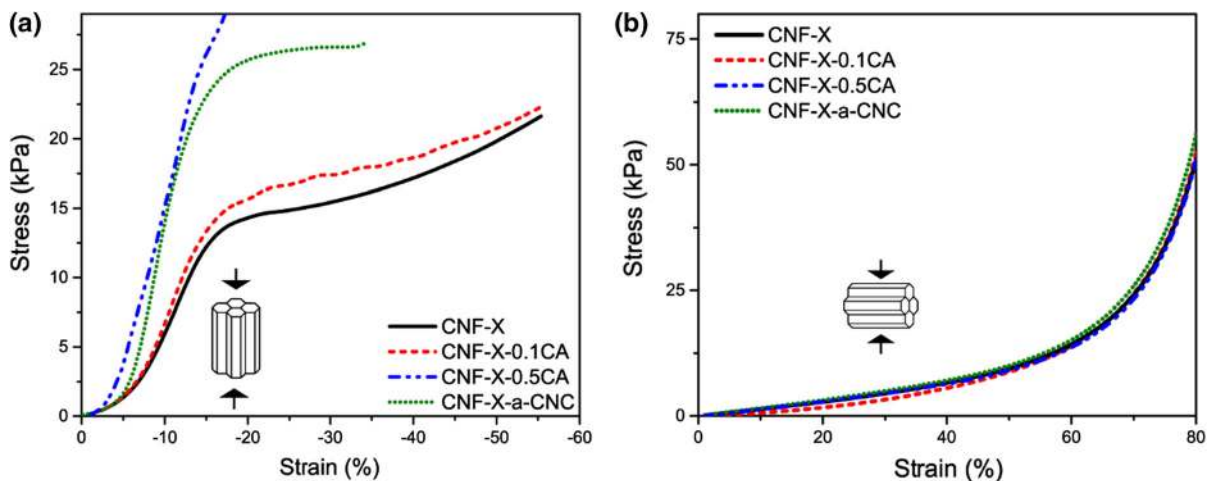

Fig. 5 Stress-strain curves of the adsorbents determined via compression tests in both **a** axial and **b** radial directions

Table 3 Elastic modulus, specific elastic modulus, and yield strength of the prepared adsorbents obtained from the compression tests in the axial direction

Samples	E (kPa)	Es (kNm/kg)	Yield strength (kPa)
CNF-X	158.2 ± 2.8	12.67	13.5 ± 0.7
CNF-X-0.1CA	172.4 ± 9.6	11.58	14.9 ± 0.9
CNF-X-0.5CA	252.7 ± 7.8	10.75	25.5 ± 0.8
CNF-X-a-CNC	328.9 ± 20.7	19.75	23.6 ± 1.7

The CO_2 adsorption properties of the adsorbents were first evaluated by adsorption isotherms measured at 273 K. Figure 6a shows the experimental data (points) and polynomials fitted to the data (curves). As shown from Fig. 6a, modified CNF-X-0.1CA and CNF-X-a-CNC adsorbed much more CO_2 than CNF-X did at a given pressure. The CO_2 adsorption capacities at 101 kPa were 1.14 mmol /g and 1.05 mmol/g for CNF-X-a-CNC and CNF-X-0.1CA, respectively. The slightly higher CO_2 adsorption capacity of CNF-X-a-CNC may be due to the nanoscale scaffold formed by the a-CNCs, which helps the aerogel to maintain more surface area after impregnation and provides more effective physisorption sites for CO_2 on the surface; this corresponded to the BET surface area data in Table 2. However, CNF-X-0.5CA only showed a slightly better specific capacity than CNF-X, which can be attributed to the decrease in surface area (less adsorption sites) and increase in density simultaneously. The decrease in surface area can be due to the filling effect of CA on the cell walls of the aerogels as discussed above, and it

can also be a result from the impregnation process where some delicate porous structure may lose.

CO_2 forward step change breakthrough experiments were also conducted to evaluate the performance of the adsorbents in an adsorption column. As shown in Fig. 6b, the measurements were conducted using a 90 kPa/10 kPa N_2/CO_2 gas mixture fed to the column under atmospheric pressure, and the CO_2 concentration at the outlet was detected. The amount of adsorbed CO_2 estimated from the breakthrough curves as illustrated in Fig. 6c should correspond to the adsorption capacity obtained from the adsorption isotherms at 10 kPa. CNF-X is considered a carrier material for functional materials because it adsorbs a very low amount of CO_2 (0.007 mmol/g) at 10 kPa, which was determined from the fitted polynomial in Fig. 6a. Therefore, the specific capacity from adsorption isotherms (q_{iso}) at 10 kPa was calculated using:

$$q_{iso} = \frac{Q_{ad} - Q_{CNF-X}}{m} \tag{6}$$

where Q_{ad} and Q_{CNF-X} are the measured adsorption capacity of the corresponding adsorbent and CNF-X,
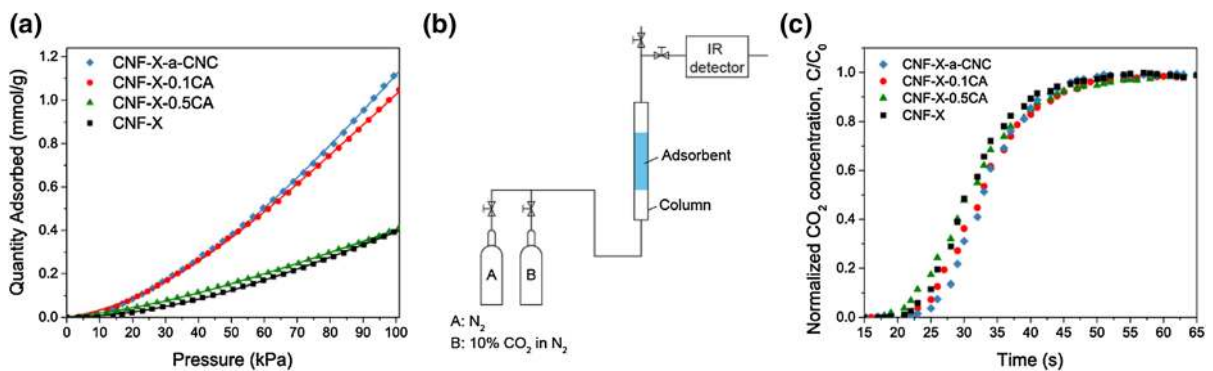

Fig. 6 **a** Experimental adsorption isotherms (points) and fitted polynomials (curves) of CNF-X-a-CNC, CNF-X-0.1CA, CNF-X-0.5CA, and CNF-X measured at 273 K in the pressure range of 0 to 101 kPa. **b** Schematic illustration of the CO_2 forward step change breakthrough equipment. **c** Forward step change breakthrough curves of CNF-X-a-CNC, CNF-X-0.1CA, CNF-X-0.5CA, and CNF-X

respectively, and m is the mass of the functional material in the adsorbent. The specific capacity from the breakthrough experiments (q_{bt}) was calculated as:

$$q_{bt} = \frac{\left(\int_{t=0}^{t=t_{ads}} \frac{v_{gas} \times (c_0 - c_1) dt}{100} \right) - A_{CNF-X}}{m} \qquad (7)$$

$$A_{CNF-X} = \int_{t=0}^{t=t_{ads}} \frac{v_{gas} \times (c_0 - c_1) dt}{100} \qquad (8)$$

where v_{gas} is the molar flow rate of the mixed N_2/CO_2 gas (mmol/s), c_0 and c_1 are the concentrations of CO_2 (vol%) in the inlet and outlet, and t_{ads} is the time when c_1/c_0 reaches 1.

Figure 7 summarizes the specific CO_2 adsorption capacity of the functional materials, *i.e.* cellulose acetate and a-CNCs, in the related adsorbents calculated from both adsorption isotherms and breakthrough measurements. It shows that the CO_2 adsorption capacity of the functional materials from both experiments has similar trends in which the a-CNCs in CNF-X-a-CNC had an approximately 45% higher CO_2 adsorption capacity than cellulose acetate did in CNF-X-0.1CA. This indicates that the use of nanomaterials to form a nano-scaffold on the surface of the aerogel provided more physisorption sites for CO_2, which contributed to the higher adsorption efficiency of a-CNCs. The cellulose acetate in CNF-X-0.5CA had the lowest specific capacity, which implied that the thicker layers formed by more cellulose acetate may not be fully accessible to CO_2. Notably, although Fig. 6a shows that the entire CNF-X-a-CNC adsorbent had a similar adsorption capacity
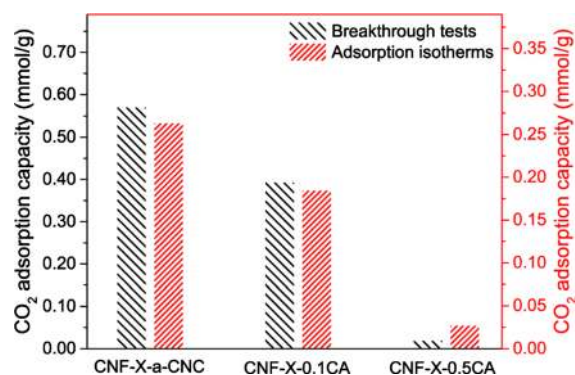

Fig. 7 CO_2 adsorption capacity of a-CNCs and cellulose acetate in the corresponding aerogels estimated from the forward step change breakthrough curves and from the adsorption isotherms

as that of CNF-X-0.1CA at 10 kPa, and the mass difference between the impregnated a-CNCs (0.07 g) and the impregnated cellulose acetate (0.1 g) caused the difference in their specific capacities.

Conclusions

Lightweight and flexible CNF-based aerogels with monolithic structures were prepared via freeze-casting. The obtained aerogels were further functionalized by being impregnated in a-CNC/acetone suspension or cellulose acetate/acetone solution. Owing to the anisotropy of the monolithic structure, the aerogels were soft and flexible in the radical direction, while the specific elastic modulus was as high as 19.75 kNm/kg in the axial direction. Introduction of acetate groups increased the affinity of the aerogels to CO_2, which allowed the functionalized aerogels to be used as CO_2 adsorbents. Unlike the cellulose acetate-forming compact layer on the surface of the aerogel, a-CNCs built a nanoscale scaffold on it. This delicate nanoscale scaffold not only significantly improved the mechanical performance of the adsorbents but also provided more physisorption sites on the aerogel; therefore, CNF-X-a-CNC had a better CO_2 adsorption capacity than CNF-X-0.1CA. Even though CNF-X-a-CNC had the highest CO_2 adsorption capacity among the adsorbents prepared in this study (1.14 mmol/g at 273 K and 101 kPa), more work is needed to make the most of this potential.

References

Abraham E, Kam D, Nevo Y, Slattegard R, Rivkin A, Lapidot S, Shoseyov O (2016) Highly modified cellulose nanocrystals and formation of epoxy-nanocrystalline cellulose (CNC) nanocomposites. ACS Appl Mater Interfaces 8:28086–28095

An J, Rosi NL (2010) Tuning MOF CO_2 adsorption properties via cation exchange. J Am Chem Soc 132:5578–5579

Arellano IH, Madani SH, Huang J, Pendleton P (2016) Carbon dioxide adsorption by zinc-functionalized ionic liquid impregnated into bio-templated mesoporous silica beads. Chem Eng J 283:692–702

Banerjee R, Furukawa H, Britt D, Knobler C, O'Keeffe M, Yaghi OM (2009) Control of pore size and functionality in isoreticular zeolitic imidazolate frameworks and their carbon dioxide selective capture properties. J Am Chem Soc 131:3875–3877

Butylina S, Geng S, Oksman K (2016) Properties of as-prepared and freeze-dried hydrogels made from poly(vinyl alcohol) and cellulose nanocrystals using freeze-thaw technique. Eur Polym J 81:386–396

Cavenati S, Grande CA, Rodrigues AE (2004) Adsorption equilibrium of methane, carbon dioxide, and nitrogen on zeolite 13X at high pressures. J Chem Eng Data 49:1095–1101

Chen B, Zheng Q, Zhu J, Li J, Cai Z, Chen L, Gong S (2016) Mechanically strong fully biobased anisotropic cellulose aerogels. RSC Adv 6:96518–96526

Deville S, Saiz E, Nalla RK, Tomsia AP (2006) Freezing as a path to build complex composites. Science 311:515–518

Fan J et al (2018) Robust nanofibrillated cellulose hydro/aerogels from benign solution/solvent exchange treatment. ACS Sustain Chem Eng 6:6624–6634

Fujiki J, Yogo K (2016) The increased CO_2 adsorption performance of chitosan-derived activated carbons with nitrogen-doping. Chem Commun 52:186–189

Gebald C, Wurzbacher JA, Tingaut P, Zimmermann T, Steinfeld A (2011) Amine-based nanofibrillated cellulose as adsorbent for CO_2 capture from air. Environ Sci Technol 45:9101–9108

Gebald C, Wurzbacher JA, Tingaut P, Steinfeld A (2013) Stability of amine-functionalized cellulose during temperature-vacuum-swing cycling for CO_2 capture from air. Environ Sci Technol 47:10063–10070

Geng S, Yao K, Zhou Q, Oksman K (2018) High-strength, high-toughness aligned polymer-based nanocomposite reinforced with ultralow weight fraction of functionalized nanocellulose. Biomacromolecules 19:4075–4083

Gibson LJ, Ashby MF (1999) Cellular solids: structure and properties. Cambridge University Press, Cambridge

Gorgieva S, Vogrinčič R, Kokol V (2019) The effect of membrane structure prepared from carboxymethyl cellulose and cellulose nanofibrils for cationic dye removal. J Polym Environ 27:318–332

Herrera MA, Mathew AP, Oksman K (2017) Barrier and mechanical properties of plasticized and cross-linked nanocellulose coatings for paper packaging applications. Cellulose 24:3969–3980

Hu W, Chen S, Xu Q, Wang H (2011) Solvent-free acetylation of bacterial cellulose under moderate conditions. Carbohydr Polym 83:1575–1581

Jonoobi M, Mathew AP, Oksman K (2014) Resources and residues for production of bionanomaterials. In: Handbook of green materials: processing technologies, properties and applications. World Scientific and Engineering Academy and Society, Singapore

Karimi S et al (2016) High flux acetate functionalized silica membranes based on in-situ co-condensation for CO_2/N_2 separation. J Membr Sci 520:574–582

Khalil HA, Bhat A, Yusra AI (2012) Green composites from sustainable cellulose nanofibrils: a review. Carbohydr Polym 87:963–979

Kilic S, Michalik S, Wang Y, Johnson JK, Enick RM, Beckman EJ (2007) Phase behavior of oxygen-containing polymers in CO_2. Macromolecules 40:1332–1341

Kongnoo A, Tontisirin S, Worathanakul P, Phalakornkule C (2017) Surface characteristics and CO_2 adsorption capacities of acid-activated zeolite 13X prepared from palm oil mill fly ash. Fuel 193:385–394

Kono H, Zakimi M (2013) Preparation, water absorbency, and enzyme degradability of novel chitin-and cellulose/chitin-based superabsorbent hydrogels. J Appl Polym Sci 128:572–581

Lee J, Deng Y (2011) The morphology and mechanical properties of layer structured cellulose microfibril foams from ice-templating methods. Soft Matter 7:6034–6040

López Durán V, Erlandsson J, Wågberg L, Larsson PA (2018) Novel, cellulose-based, lightweight, wet-resilient materials with tunable porosity, density, and strength. ACS Sustain Chem Eng 6:9951–9957

Millward AR, Yaghi OM (2005) Metal–organic frameworks with exceptionally high capacity for storage of carbon dioxide at room temperature. J Am Chem Soc 127:17998–17999

Nissilä T, Hietala M, Oksman K (2019) A method for preparing epoxy-cellulose nanofiber composites with an oriented structure. Compos Part A Appl Sci Manuf 125:105515

Ojuva A, Akhtar F, Tomsia AP, Bergström L (2013) Laminated adsorbents with very rapid CO_2 uptake by freeze-casting of zeolites. ACS Appl Mater Interfaces 5:2669–2676

Oksman K, Skrifvars M, Selin JF (2003) Natural fibres as reinforcement in polylactic acid (PLA) composites. Compos Sci Technol 63:1317–1324

Park HB, Lee YM (2008) Polymeric membrane materials and potential use in gas separation. In: Advanced membrane technology and applications. Wiley, Hoboken, pp 633–669

Pino L, Italiano C, Vita A, Fabiano C, Recupero V (2016) Sorbents with high efficiency for CO_2 capture based on amines-supported carbon for biogas upgrading. J Environ Sci 48:138–150

Ramírez JAÁ, Fortunati E, Kenny JM, Torre L, Foresti ML (2017) Simple citric acid-catalyzed surface esterification of cellulose nanocrystals. Carbohydr Polym 157:1358–1364

Rezaei F, Webley P (2010) Structured adsorbents in gas separation processes. Separation Purification Technology 70:243–256

Roberts AD, Lee J-SM, Wong SY, Li X, Zhang H (2017) Nitrogen-rich activated carbon monoliths via ice-templating with high CO_2 and H_2 adsorption capacities. J Mater Chem A 5:2811–2820

Salehi S, Anbia M (2017) High CO_2 adsorption capacity and CO_2/CH_4 selectivity by nanocomposites of MOF-199. Energy Fuels 31:5376–5384

Sehaqui H, Zhou Q, Berglund LA (2011) High-porosity aerogels of high specific surface area prepared from nanofibrillated cellulose (NFC). Compos Sci Technol 71:1593–1599

Singh G, Kim IY, Lakhi KS, Srivastava P, Naidu R, Vinu A (2017) Single step synthesis of activated bio-carbons with a high surface area and their excellent CO_2 adsorption capacity. Carbon 116:448–455

Svec F, Huber CG (2006) Monolithic materials: promises, challenges, achievements. Anal Chem 78:2100–2107

Uschanov P, Johansson L-S, Maunu SL, Laine J (2011) Heterogeneous modification of various celluloses with fatty acids. Cellulose 18:393–404

Valencia L, Rosas-Arbelaez W, Aguilar-Sánchez A, Mathew AP, Palmqvist AE (2019) Biobased micro/meso/macroporous hybrid foams with ultra-high zeolite loadings for selective capture of carbon dioxide. ACS Appl Mater Interfaces 11:40424–40431

Yang J, Xia Y, Xu P, Chen B (2018) Super-elastic and highly hydrophobic/superoleophilic sodium alginate/cellulose aerogel for oil/water separation. Cellulose 25:3533–3544

Yu C-H, Huang C-H, Tan C-S (2012) A review of CO_2 capture by absorption and adsorption. Aerosol Air Qual Res 12:745–769

Zhang X, Wang H, Cai Z, Yan N, Liu M, Yu Y (2019) Highly compressible and hydrophobic anisotropic aerogels for selective oil/organic solvent absorption. ACS Sustain Chem Eng 7:332–340

Zhou X et al (2016) Effect of the degree of substitution on the hydrophobicity of acetylated cellulose for production of liquid marbles. Cellulose 23:811–821